NAVAL AIR WARFARE CENTER AIRCRAFT DIVISION
PATUXENT RIVER, MARYLAND

TECHNICAL REPORT

REPORT NO: NAWCADPAX/TR-2007/4

MODE I AND MODE II INTERLAMINAR CRACK GROWTH RESISTANCES OF CERAMIC MATRIX COMPOSITES AT AMBIENT TEMPERATURE

by

Sung R. Choi
Robert W. Kowalik
Donald J. Alexander

2 March 2007

DEPARTMENT OF THE NAVY
NAVAL AIR WARFARE CENTER AIRCRAFT DIVISION
PATUXENT RIVER, MARYLAND

NAWCADPAX/TR-2007/4
2 March 2007

MODE I AND MODE II INTERLAMINAR CRACK GROWTH RESISTANCES OF CERAMIC MATRIX COMPOSITES AT AMBIENT TEMPERATURE

by

Sung R. Choi
Robert W. Kowalik
Donald Alexander

RELEASED BY:

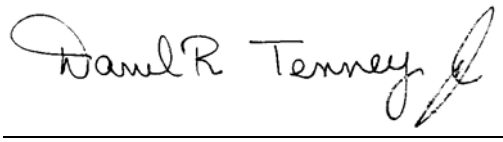

2 Mar 2007

DARREL TENNEY / 4.3.4.1 / DATE
Head, Metals and Ceramics Branch
Naval Air Warfare Center Aircraft Division

REPORT DOCUMENTATION PAGE

Form Approved
OMB No. 0704-0188

1. REPORT DATE	2. REPORT TYPE	3. DATES COVERED
2 March 2007	Technical Report	FY06

4. TITLE AND SUBTITLE	5a. CONTRACT NUMBER
Mode I and Mode II Interlaminar Crack Growth Resistances of Ceramic Matrix Composites at Ambient Temperature	5b. GRANT NUMBER
	5c. PROGRAM ELEMENT NUMBER
6. AUTHOR(S) Sung R. Choi Robert W. Kowalik Donald Alexander	5d. PROJECT NUMBER
	5e. TASK NUMBER
	5f. WORK UNIT NUMBER
7. PERFORMING ORGANIZATION NAME(S) AND ADDRESS(ES) Naval Air Warfare Center Aircraft Division 22347 Cedar Point Road, Unit #6 Patuxent River, Maryland 20670-1161	8. PERFORMING ORGANIZATION REPORT NUMBER NAWCADPAX/TR-2007/4
9. SPONSORING/MONITORING AGENCY NAME(S) AND ADDRESS(ES) Naval Air Systems Command 47123 Buse Road Unit IPT Patuxent River, Maryland 20670-1547	10. SPONSOR/MONITOR'S ACRONYM(S)
	11. SPONSOR/MONITOR'S REPORT NUMBER(S)

12. DISTRIBUTION/AVAILABILITY STATEMENT

Approved for public release; distribution is unlimited.

13. SUPPLEMENTARY NOTES

14. ABSTRACT

Interlaminar crack growth resistances were determined for five different SiC fiber-reinforced ceramic matrix composites (CMCs) including three gas-turbine grade melt-infiltrated SiC/SiC composites. Modes I and II crack growth resistances, G_I and G_{II}, were evaluated at ambient temperature using double cantilever beam and end notched flexure methods, respectively. The CMCs exhibited G_I =200-500 J/m^2 and G_{II}=200-900 J/m^2. Most of the CMCs, except the SiC/CAS composite, showed rising R-curve behavior either in Mode I or in Mode II, presumably attributed to fiber bridging (in Modes I and II) and frictional constraint (in Mode II) in the wake region of a propagating crack. A glass fiber-reinforced epoxy polymer matrix composite, used as comparison, showed R-curve behavior and typically 2-3 and 8 times greater in G_I and G_{II}, respectively, than the CMCs. Experimental error analysis concerning the effect of the off-the-center of a crack plane on G_I and G_{II} was also made.

15. SUBJECT TERMS

Ceramic matrix composites (CMCs); crack growth resistances, interlaminar properties; mechanical properties; Mode I and Mode II energy release rates

16. SECURITY CLASSIFICATION OF:			17. LIMITATION OF ABSTRACT	18. NUMBER OF PAGES	19a. NAME OF RESPONSIBLE PERSON
a. REPORT	b. ABSTRACT	c. THIS PAGE			Sung R. Choi
Unclassified	Unclassified	Unclassified	SAR	40	19b. TELEPHONE NUMBER (include area code); EMAIL 301-342-8009; sung.choi1@navy.mil

Standard Form 298 (Rev. 8-98)
Prescribed by ANSI Std. Z39-18

SUMMARY

Interlaminar crack growth resistances were determined for five different SiC fiber-reinforced ceramic matrix composites (CMCs) including three gas-turbine grade melt-infiltrated SiC/SiC composites. Modes I and II crack growth resistances, G_I and G_{II}, were evaluated at ambient temperature using double cantilever beam and end notched flexure methods, respectively. The CMCs exhibited G_I =200-500 J/m^2 and G_{II}=200-900 J/m^2. Most of the CMCs, except the SiC/CAS composite, showed rising R-curve behavior either in Mode I or in Mode II, presumably attributed to fiber bridging (in Modes I and II) and frictional constraint (in Mode II) in the wake region of a propagating crack. A glass fiber-reinforced epoxy polymer matrix composite, used as comparison, showed R-curve behavior and typically 2-3 and 8 times greater in G_I and G_{II}, respectively, than the CMCs. Experimental error analysis concerning the effect of the off-the-center of a crack plane on G_I and G_{II} was also made.

Contents

ACKNOWLEDGEMENTS

The authors would like to acknowledge the Office of Naval Research and Dr. D. Shifler for the support of this work.

1. INTRODUCTION

The successful development and design of continuous fiber-reinforced ceramic matrix composites (CMCs) are dependent on understanding their basic mechanical properties such as deformation, strength, fracture resistance, and delayed failure (fatigue, slow crack growth, or stress rupture) associated with temperature/environment. Although fiber-reinforced CMCs have shown improved resistance to fracture and increased damage tolerance compared with the monolithic ceramics, inherent material/processing defects or cracks in the matrix-rich interlaminar and/or interface regions can still cause delamination under interlaminar normal or shear stress, resulting in loss of stiffness or, in some cases, structural failure [1-4]. CMCs also have shown life limiting susceptibility even in interlaminar shear particularly at elevated temperatures, resulting in time-dependent strength degradation or shortening of component life [5-6].

In a previous study [7], both interlaminar tensile and shear strengths were determined for six different SiC fiber-reinforced CMCs at ambient temperature. The CMCs, 2-D woven or cross-plied, exhibited poor interlaminar properties with interlaminar shear strength of 30-50 MPa and interlaminar tensile strength of 10-20 MPa. Interlaminar shear strength was two to three times greater than the interlaminar (or transthickness) tensile strength [7-10], implying a difference in the crack growth resistance between Modes I and II loading. Several approaches to improve interlaminar properties of CMCs are under way through architectural modifications such as "2.5"- or 3-D weave or through matrix-material modifications. However, almost no work has been done to determine systematically and simultaneously Mode I and Mode II interlaminar crack growth resistances of even conventional 1-D or 2-D CMCs. Only limited data are found for CMCs from the literature [11]. This contrasts with polymer matrix composites (PMCs), where extensive data, as well as analytical work on crack growth resistance, have been found and accumulated for several decades [12-18].

The purpose of this work was to determine systematically both Modes I and II crack growth resistances (G_{I} and G_{II}) at ambient temperature for five different SiC fiber-reinforced CMCs, including three gas-turbine grade melt-infiltrated (MI) SiC/SiC composites. Crack growth resistances G_{I} and G_{II} were evaluated with the compliance approach using double cantilever beam (DCB) and end notched flexure (ENF) methods, respectively. A 2-D woven glass fiber-reinforced epoxy matrix composite and a superglued polymethyl methacrylate (PMMA) were also used for comparison. The microstructural aspects of the CMCs were characterized to better understand mechanisms related to crack propagation under different modes of loading. Experimental error analysis concerning the effect of the off-the-center of a crack plane on crack growth resistances was also made. Some of this work was reported previously [19].

2. EXPERIMENTAL PROCEDURES

2.1 MATERIALS

Five different SiC fiber-reinforced CMCs, four SiC/SiCs and one SiC/glass ceramic, were used in this work. These include 2-D woven MI Hi-Nicalon™ fiber-reinforced SiC (designated Hi-Nic SiC/SiC), 2-D woven MI Sylramic™ fiber-reinforced SiC (designated S-SiC/SiC), 2-D woven MI Nicalon™ fiber-reinforced SiC (designated U-SiC/SiC), 2-D plain-woven Nicalon™ fiber-reinforced SiC (designated SiC/SiC ('90)), and 1-D Nicalon™ fiber-reinforced calcium aluminosilicate (designated SiC/CAS). Note that Hi-Nic SiC/SiC, S-SiC/SiC, and U-SiC/SiC were for gas-turbine grade CMCs with upper temperature limits of 1200-1300^{o}C [20,21]. For comparison, a 2-D woven glass-fiber reinforced epoxy PMC and PMMA were also used. Basic information on preform descriptions and resulting laminates of the CMCs and on PMC and PMMA is summarized in table 1. Elastic moduli of the materials are also included.

Table 1: Continuous Fiber-Reinforced CMCs, PMC, and PMMA Used in this Work

	Materials	Architecture	Fiber[#]	Fiber Volume Fraction	Process and Laminates[†]	Elastic Modulus, E (GPa)*	Manufacturer
1	Hi-Nic SiC/SiC ('02)	2-D woven	Hi-Nic™ SiC[*]	0.39	iBN;SC/MI;5HS; 8 ply,t=2.1mm;20epi	183	GEPSC[***]
2	S-SiC/SiC ('01)	2-D woven	Sylramic™ SiC[**]	0.39	iBN;SC/MI;5HS;8 ply,t=2.5mm;20epi	222	GEPSC
3	U-SiC/SiC ('02)	2-D woven	Nicalon™ SiC[*]	0.39	iBN;SC/MI;5HS;8 ply,t=2.1mm;20epi	195	GEPSC
4	SiC/SiC ('90)	2-D woven	Nicalon™ SiC[*]	0.39	CVI;plain;12ply; t=3.4mm	215	E.I.Du Pont
5	SiC/CAS ('90)	Unidirectional (1-D)	Nicalon™ SiC[*]	0.39	HP;18 ply;t=3.4 mm	137	Corning
6	Glass/epoxy PMC	2-D woven	Glass	0.30[§]	30 ply;t=6.3 mm	23	–
7	PMMA	–	–	–	t=6.5 mm; two PMMA beams superglued	5	–

[*] Nippon Carbon (Japan); [**] Dow Corning (Midland, MI); [***] General Electric Power System Composites (Newark, DL)

† BN: boron nitride; SC: slurry casting; MI: melt infiltration; HS: harness satin; CVI: chemical vapor infiltration; HP: hot pressed; epi: ends per inch; *t* (=2*h*): as-fabricated thickness.

* Elastic modulus E (in-plane) was determined by the impulse excitation of vibration technique, ASTM C 1259 [22].

§ Estimated based on the rule-of-mixture with E=70 GPa for glass fibers and E=4 GPa for epoxy.

[#] SiC fibers of CMCs 1 to 3 were BN coated while SiC fibers of CMCs 4 to 5 were uncoated (see also microstructures in figure 1).

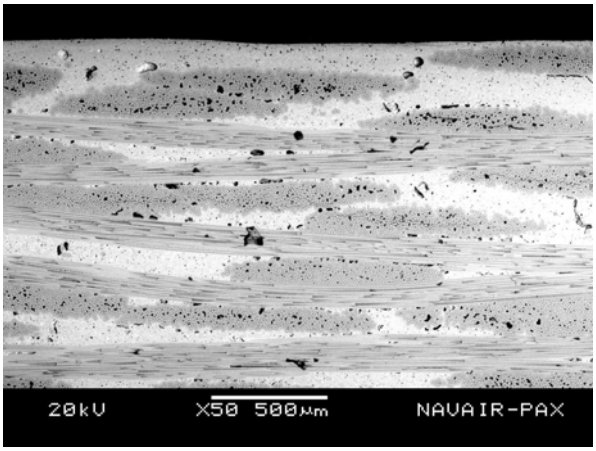

(a) Hi-Nic SiC/SiC

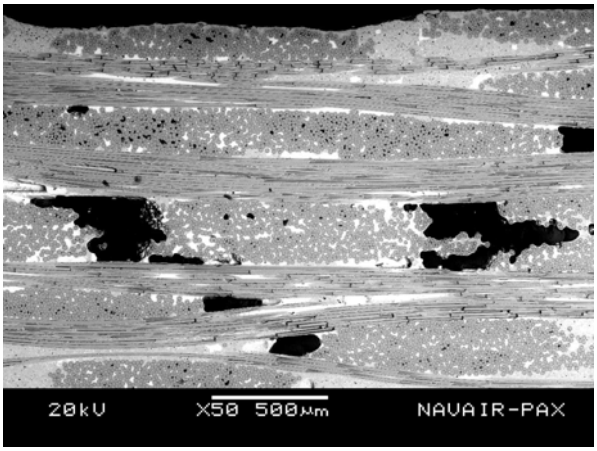

(b) S-SiC/SiC

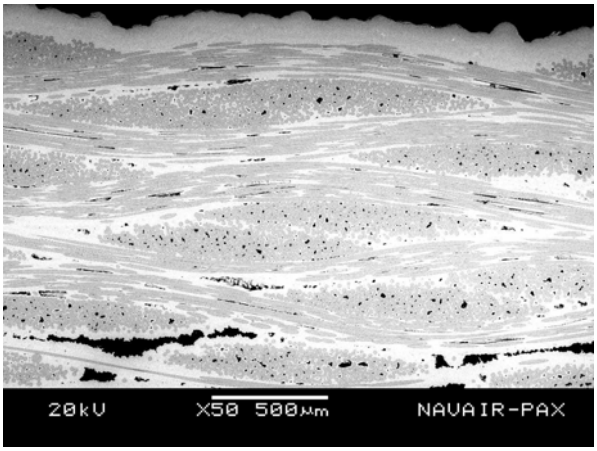

(c) U-SiC/SiC

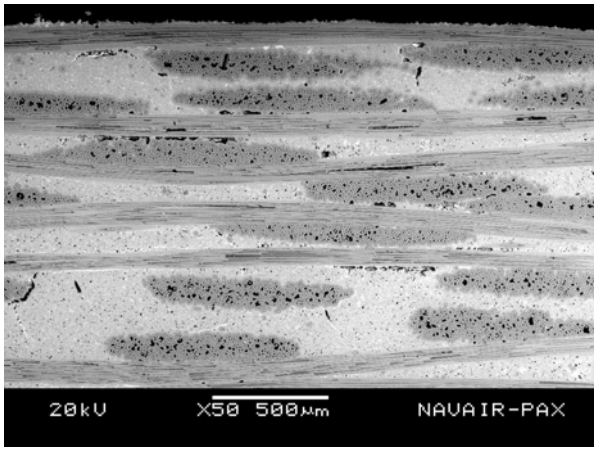

(d) SiC/SiC (’90)

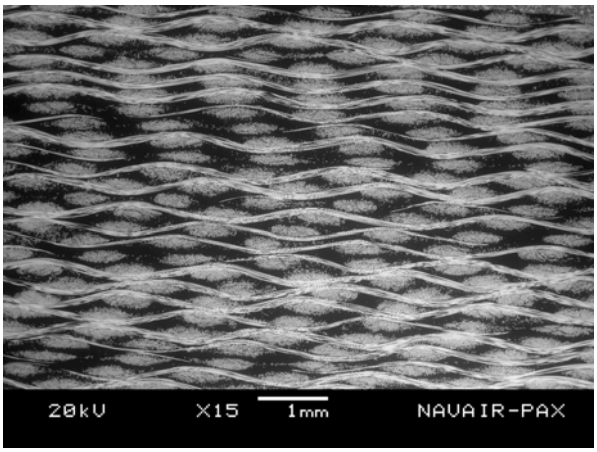

(e) SiC/CAS

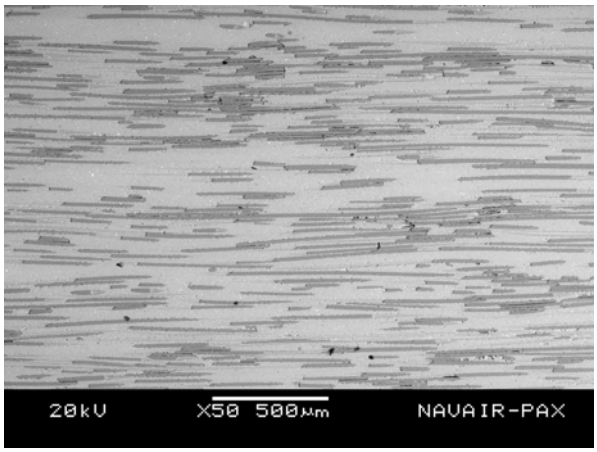

(f) PMC (glass/epoxy)

Figure 1: Microstructures of test materials used in this work: (a) 2-D woven Hi-Nic SiC/SiC, (b) 2-D woven S-SiC/SiC, (c) 2-D woven U-SiC/SiC, (d) 2-D woven SiC/SiC (’90), (e)1-D SiC/CAS, and (f) 2-D woven glass/epoxy PMC.

Briefly, the fiber cloth preforms in the MI SiC/SiC composites were stacked and chemically vapor infiltrated with a thin BN-based interface coating followed by SiC matrix over-coating. Remaining matrix porosity was filled with SiC particulates and then with molten silicon at 1400^{o}C, a process termed slurry casting (SC) and MI [20]. Details regarding processing of these CMCs can be found elsewhere [20]. The silicon carbide matrix in the SiC/SiC (’90) composite was processed through CVI into the fiber preforms. The SiC/CAS composite was fabricated via hot pressing followed by ceraming of the composite by a thermal process [23]. Some of the CMS used in this work have been employed previously for determinations of time-dependent in-plane tensile and interlaminar shear strength behaviors at elevated temperatures [6,7,24], foreign object damage behavior [25], and of interlaminar shear and tensile properties at ambient temperature [7].

Microstructure of each of the composites is shown in figure 1. The Hi-Nic SiC/SiC, S-SiC/SiC, and U-SiC/SiC composites showed interfacial BN coatings while no coating was observed for the SiC/SiC (’90) and SiC/CAS composites. Average fiber diameter was in a range of 10 to 15 μm for the Hi-Nic SiC/SiC, S-SiC/SiC, and U-SiC/SiC composites, 12-18 μm for the SiC/SiC (’90) and SiC/CAS composites, and 6 to 8 μm for the PMC. MI silicon was also seen in matrices and interfaces of the Hi-Nic SiC/SiC, S-SiC/SiC, and U-SiC/SiC composites.

2.2 INTERLAMINAR MODE I AND MODE II TESTS

Modes I and II crack growth resistances (or called ‘energy release rates’, used interchangeably in this paper) of the CMCs were determined at ambient temperature in air by using DCB and ENF methods, respectively. The nominal dimensions of both Modes I and II test specimens were typically L=50 mm in length, b=10-13 mm in width, and t=2h=2.1-3.4 mm in thickness (see figure 2). The thickness of test specimens was the same as the as-fabricated, nominal thickness of each CMC panel (see table 1).

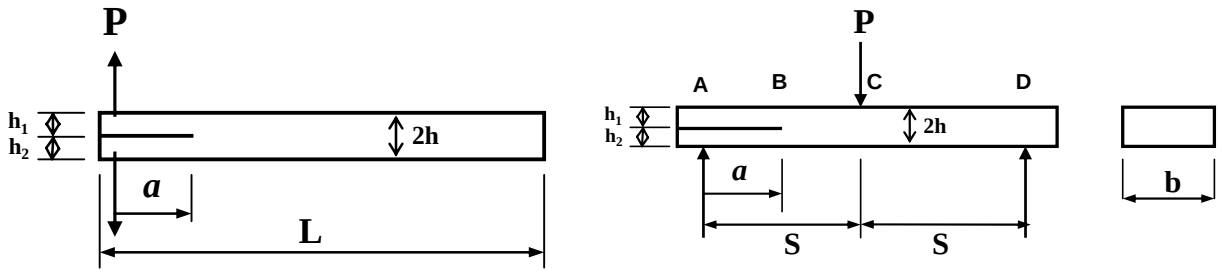

Figure 2: Schematics of test specimen/loading configurations used in (a) DCB test for Mode I and (b) ENF test for Mode II.

A precrack was generated at one end of each test specimen along its interlaminar midplane using a specially designed precrack fixture together with a razor blade. Propagation of precracks in the 1-D SiC/CAS composite were along with the fiber direction. Typical crack length used was $a \geq 10$ mm either in DCB test specimens or in ENF test specimens. Each DCB test specimen precracked was loaded by a test frame at 0.25 mm/min in displacement control via two pin-loaded grips. Crack propagation and crack mouth opening displacement (COD) were monitored using a traveling telescope and an extensometer, respectively. Force, crack length, and COD of each test specimen were in situ recorded during testing through a data acquisition system. For ENF testing, each specimen was loaded in three-point flexure with a span length of $2S=40$ mm (see figure 2) at 0.25 mm/min via the test frame that was used in DCB testing. Deflection of each test specimen at the load point was determined using a linear variable capacitance transducer and crack length was determined using the traveling telescope as well. Crack length measurements in DCB or ENF testing were greatly enhanced by using a thin coat of white correction fluid applied to both sides of each test specimen. Typically, for a given material, a total of three to five test specimens were used for each test method. The DCB and ENF methods have been widely used to determine G_{I} and G_{II} of many unidirectional fiber-reinforced PMCs, although their recommended 'precracking' procedure [26] is different from that used in this work for CMCs.

Additional ENF compliance testing was performed to determine compliances of test specimens with cracks grown in Mode I loading. A crack in each test specimen was grown in Mode I wedge loading and corresponding compliance was determined as a function of crack length in three-point ENF flexure. This testing was primarily to compare compliance of test specimen between the two modes (Mode I and Mode II) of cracking. One test specimen was utilized for each material.

The nominal dimensions of the glass/epoxy PMC used for comparison in Modes I and II tests were typically $L=50$ mm, $b=11$ mm, and $t=2h=6.3$ mm. In one case in Mode I test, the nominal dimensions were greater ($L=75$ mm and $b=20$ mm) than the typical to see any size effect on crack growth resistances. The precrack and test procedures were the same as those used for the CMCs. Two as-fabricated (polished quality) PMMA beams, each typically measured $L \geq 50$ mm, $b=13$ mm, and $t=3.2$ mm, were bonded together, interface-delaminated, and subjected to Modes I and II tests. The mating surfaces of the PMMA beams were cleaned with alcohol, dried, and glued together with a few drops of superglue (cyanoacrylate). The precrack (delaminated) and test procedures for PMMA were the same as those used for the CMCs but with one exception, which was a test rate of 0.5 mm/min. The test method used for PMMA in Mode I was similar in principle to the techniques applied for adhesion tests of various coatings on substrates such as thin metallic or polymeric films and thermal barrier coatings, etc. [27,28].

3. RESULTS AND DISCUSSION

3.1 FORMULATIONS OF CRACK GROWTH RESISTANCES

In the compliance method, crack growth resistance (or 'energy release rate') in either Mode I or Mode II can be expressed as follows [29]:

$$G_I, G_{II} = \frac{P^2}{2b}\frac{\partial C}{\partial a} \tag{1}$$

where G_I and G_{II} are energy release rate in Mode I and II, respectively. P is applied force, b is test specimen's width (see figure 2), and a is crack length. The compliance of a specimen, C, is defined as

$$C = \frac{\delta}{P} \tag{2}$$

where δ is displacement, i.e., COD in Mode I or beam deflection at the load point in Mode II. This compliance method has been used to evaluate interlaminar crack growth resistance or interlaminar fracture toughness of PMCs [12-16,18,26]. Equation (1) can be further simplified using appropriate compliance relations based on the simple beam theory, pertinent to each of the specimen/loading configurations given in figure 2, as follows:

$$G_I = \frac{3P^2C^{2/3}}{2A_1bh} \tag{3}$$

$$G_{II} = \frac{9a^2P^2C}{2b(2S^3 + 3a^3)} \tag{4}$$

which is the case for $h_1=h_2=h=t/2$. In either expression, the compliance C can be determined from force versus COD curves in Mode I (DCB) and force versus deflection curves in Mode II (ENF). The constant A_1 is a slope in the relation of normalized crack length (a/t) versus compliance ($C^{1/3}$), determined by a linear regression analysis. Equation (3) is one formulae recommended in ASTM D 5528 [26]. There are several different expressions of G_I or G_{II} in the literature but they are essentially the same but only in different forms. Equations (3) and (4) are based on the assumptions that two cantilever beams are rigidly fixed at their ends in DCB test specimens, and that no shear deformation occurs in ENF test specimens. These assumptions are more relevant to CMCs test specimens for their thin configurations and much higher elastic modulus, as compared to PMCs (see elastic modulus in table 1). There are also modifications in G_I to account for large deformation of test specimens, applied to compliant PMCs [26].

3.2 MODE I INTERLAMINAR CRACK RESISTANCE

A typical example of force versus COD curves determined for the SiC/SiC ('90) composite in Mode I is depicted in figure 3. Linearity existed between force and COD for a given crack length. Crack growth occurred after reaching the peak force in the linear region, followed by an increase in compliance with subsequent loading. The inverse of slope of each curve for a given crack length gives a value of compliance. Results of crack length (a/t) as a function of compliance ($C^{1/3}$) for all the materials tested are shown in figure 4. A linear relationship between the two related parameters holds with the coefficients of correlation of curve fit all greater than r_{coef} >0.99. This linearity validates the use of Equation (3). However, some scatter, as seen in the figure, was inevitable among test specimens particularly for the CMCs, implying the existence of certain degree of material's inhomogeneity. Note that as aforementioned, the value of A_1 can be obtained in figure 4 from the slope of each curve for a given material. The scatter shown in the a/t *versus* $C^{1/2}$ relations was also reflected in the value of A_1, as shown in figure 5, in which A_1 was compared with the calculated A_1.

$$A_{1cal} = \frac{[Eb]^{1/3}}{4} \tag{5}$$

Equation (5) is based on the simple beam theory and E is elastic modulus listed in table 1. The PMC and PMMA exhibited good agreement between the experimental and the calculated A_1's while some of the CMCs showed a deviation. This indicates that use of the calculated A_1 would not be appropriate in G_I estimation, attributed to the inhomogeneous nature of the materials. Therefore, the use of the slope as A_1 from each a/t *versus* $C^{1/3}$ curve is preferred, as also recommended in ASTM D 5528 [26].

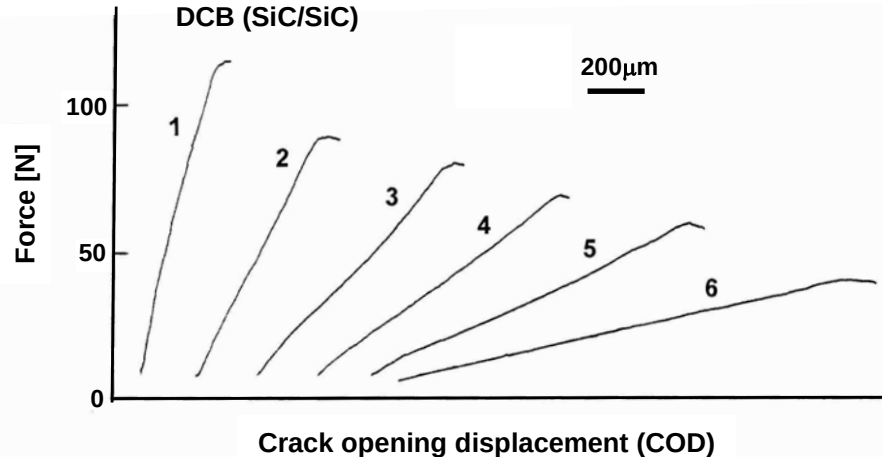

Figure 3: Typical force versus displacement curve determined in DCB (Mode I) test for SiC/SiC ('90). Each curve numbered represents one loading(/unloading) sequence for a given crack length.

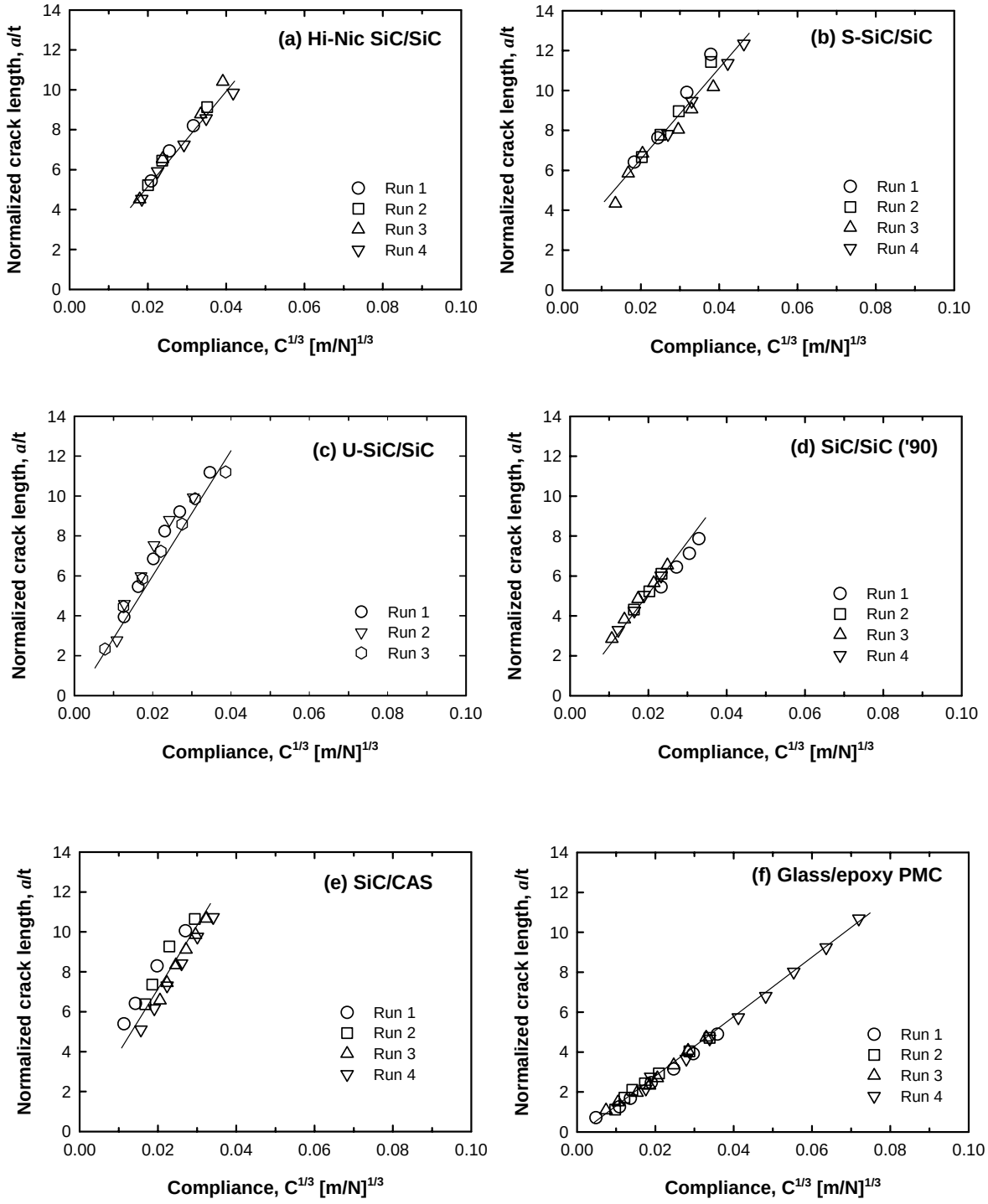

Figure 4: Normalized crack length (a/t) as a function of compliance ($C^{1/3}$) determined at ambient temperature by DCB in Mode I for (a) Hi-Nic SiC/SiC, (b) S-SiC/SiC, (c) U-SiC/SiC, (d) SiC/SiC (’90), (e) SiC/CAS, (f) glass/epoxy PMC, and (g) PMMA (superglued).

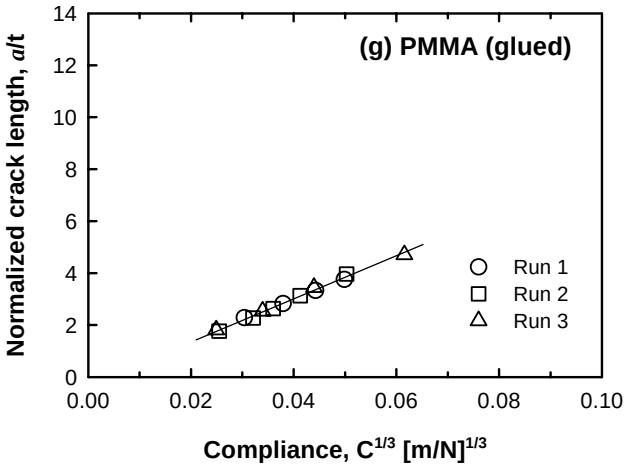

Figure 4: (Cont'd)

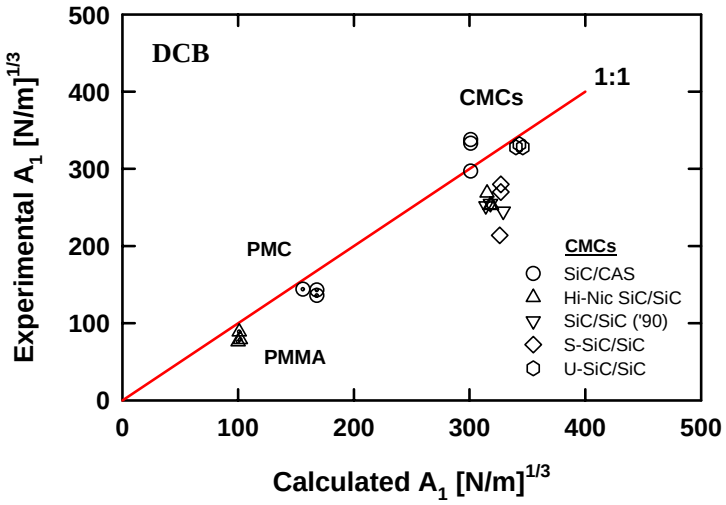

Figure 5: Comparison in A_1 between the experimental and calculated values for five different CMCs, PMC, and PMMA tested in Mode I.

A summary of Mode I interlaminar energy release rate G_I is shown in figure 6, where G_I was plotted as a function of crack length (a). Except for the SiC/CAS composite, G_I increased with increasing crack length, termed R-curve behavior, ranging from 200 to 500 J/m^2. G_I was greatest for the Hi-Nic SiC/SiC composite and appeared to be similar for the other three SiC/SiC composites. The unidirectionally (1-D) reinforced SiC/CAS composite exhibited a flat R-curve with a value of $G_I \approx 150$ J/m^2 and showed much less scatter in data as compared with other CMCs.

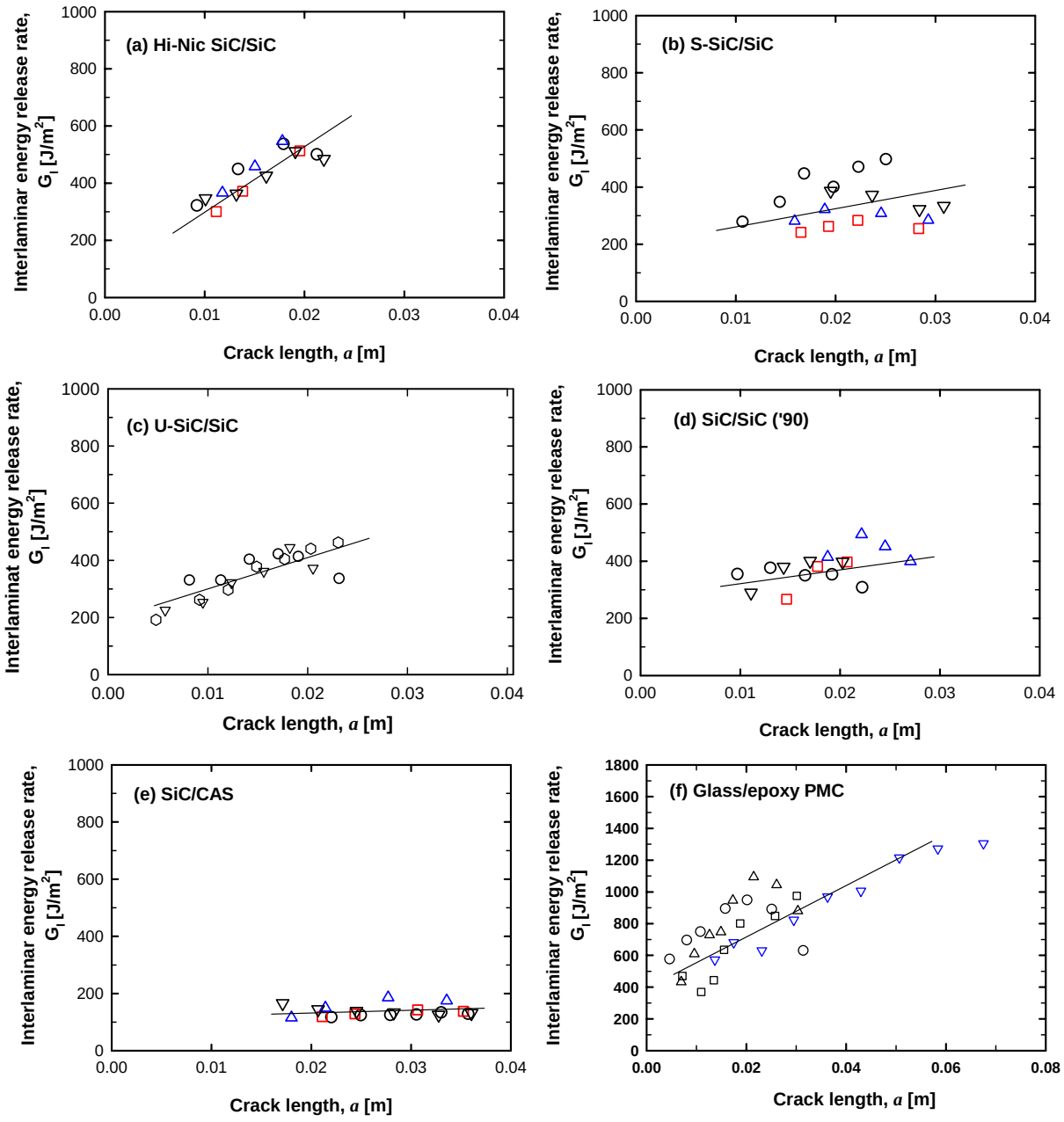

Figure 6: Mode I interlaminar energy release rate (G_I) as a function of crack length determined at ambient temperature by DCB in Mode I for (a) Hi-Nic SiC/SiC, (b) S-SiC/SiC, (c) U-SiC/SiC, (d) SiC/SiC (’90), (e) SiC/CAS, (f) glass/epoxy PMC, and (g) PMMA (superglued). Each symbol represents a test run for a given specimen.

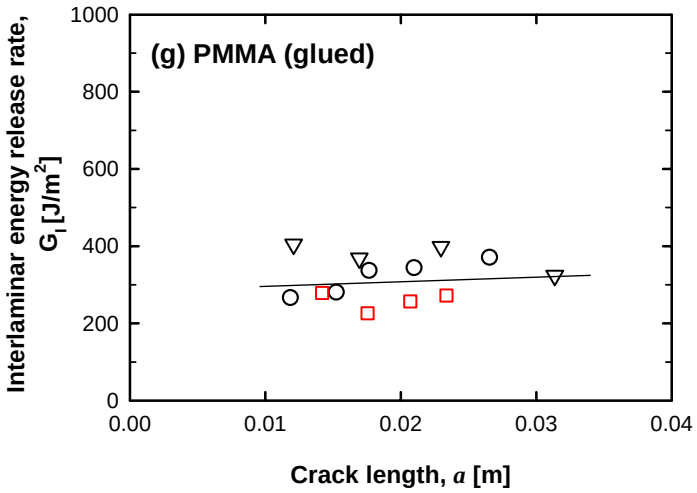

Figure 6: (Cont'd)

The glass/epoxy composite showed significant G_I ranging from 400 to 1200 J/m^2 with a rising R-curve. Also the composite revealed little size effect on G_I, either with the regular dimensions (L=50 mm; b=11 mm) or with the larger ones (L=75 mm; b=20 mm). PMMA exhibited $G_I \approx 300$ N/m^2 with a flat R-curve.

3.3 MODE II INTERLAMINAR CRACK RESISTANCE

It was experienced to be more difficult to conduct Mode II ENF tests than Mode I DCB counterparts since, in some cases, undesirable *flexure* failure occurred in ENF specimens before a crack propagated. It was also observed that a crack, when approaching the load point, tended to deviate from the midplane toward the outside surface of an ENF specimen. Flexure failure was able to be mitigated using an initial precrack size of $a \geq (0.4\text{-}0.5)S$, where a crack driving energy (G_{II}) would be greater than a flexure-fracture inducing energy. As a result, ENF test method was found to be effective in a range of $0.5 \leq a/S < 1.0$ for the materials used in this work.

A typical example of force versus center deflection curves in Mode II is presented in figure 7. A linear relationship existed between force and center deflection for a given crack length. Crack growth took place after reaching the peak force in the linear region, followed by an increase in compliance with subsequent loading. Results of compliance (C) versus normalized crack length $(a/S)^3$ for the materials tested are shown in figure 8. Overall, C versus $(a/S)^3$ showed a reasonably good linearity with the coefficients of correlation of $r_{coef} \geq 0.90$. This linearity again would justify the use of Equation (4). However, as seen in the case of Mode I, some scatter in curves was also inevitable in Mode II among test specimens for a given material, indicative of material's inhomogeneity.

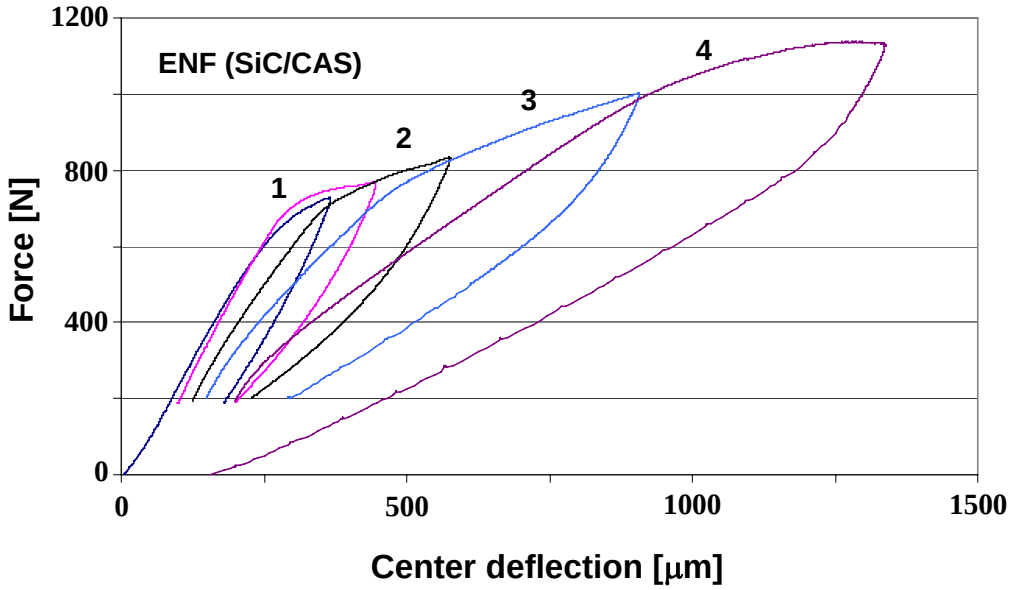

Figure 7: Typical force versus displacement curve determined in ENF (Mode II) test for SiC/CAS. Each curve numbered represents one loading(/unloading) sequence for a given crack length.

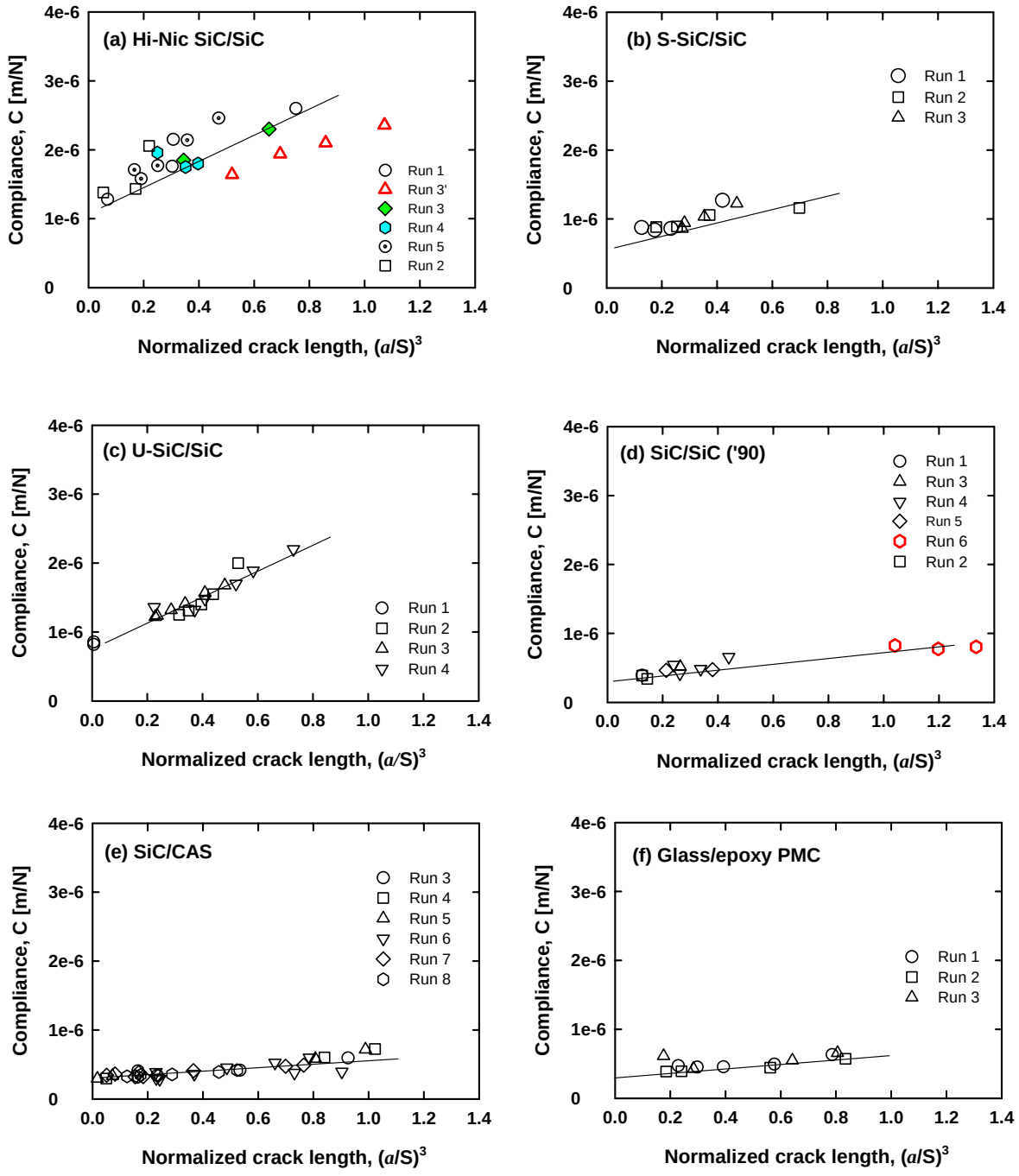

Figure 8: Compliance (C) as a function of normalized crack length $(a/S)^3$ determined at ambient temperature by ENF in Mode II for (a) Hi-Nic SiC/SiC, (b) S-SiC/SiC, (c) U-SiC/SiC, (d) SiC/SiC ('90), (e) SiC/CAS, (f) glass/epoxy PMC, and (g) PMMA (superglued).

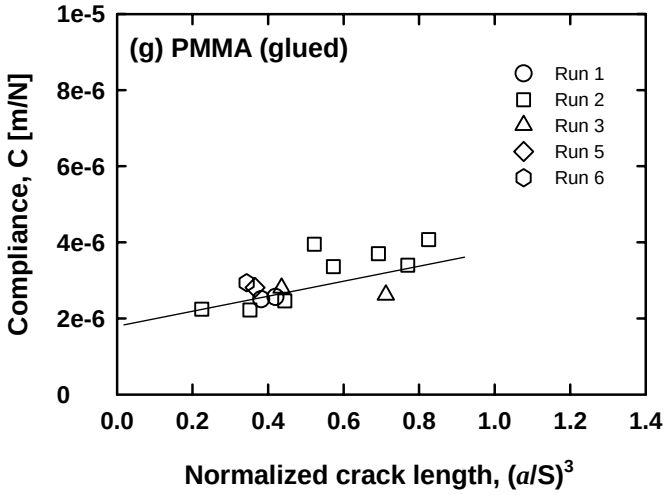

Figure 8: (Cont'd)

Results of the additional compliance testing are also depicted in figure 9 (as a data symbol of "Compl. check"). It appears that no appreciable difference existed in compliance of test specimens with either Mode I or Mode II grown cracks. This, however, does not necessarily mean that crack growth resistance would remain the same between the two different crack systems, since subsequent crack growth resistance would depend on morphological/architectural features of two mating crack planes such as fiber bridging, surface roughness, friction, etc. In principle, the intercept of the C versus $(a/S)^3$ curves in figure 9 (or 8) corresponds to the compliance (C_o) of a test specimen with zero crack length. The compliance C_o is simply from the beam theory

$$C_o = \frac{S^3}{4Ebh^3} \tag{6}$$

which can be calculated with elastic modulus and specimen/fixture geometries. Also, following the procedure done by Carlsson et al.[14], the ratio of C to C_o yields

$$\frac{C}{C_o} = 1 + 1.5\,(\frac{a}{S})^3 \tag{7}$$

Figure 10 depicts normalized compliance (C/C_o) as a function of $(a/S)^3$ and compares it with the calculated based on Equation (7). Although the materials generally follow the idealized case of Equation (7), they exhibited some deviations in C/C_o between the experimental and the calculated, indicating again the inhomogeneous nature of the materials. Therefore, the use of individual experimental values of compliance should be used in estimating crack growth resistance (G_{II}), as directed in Equation (4).

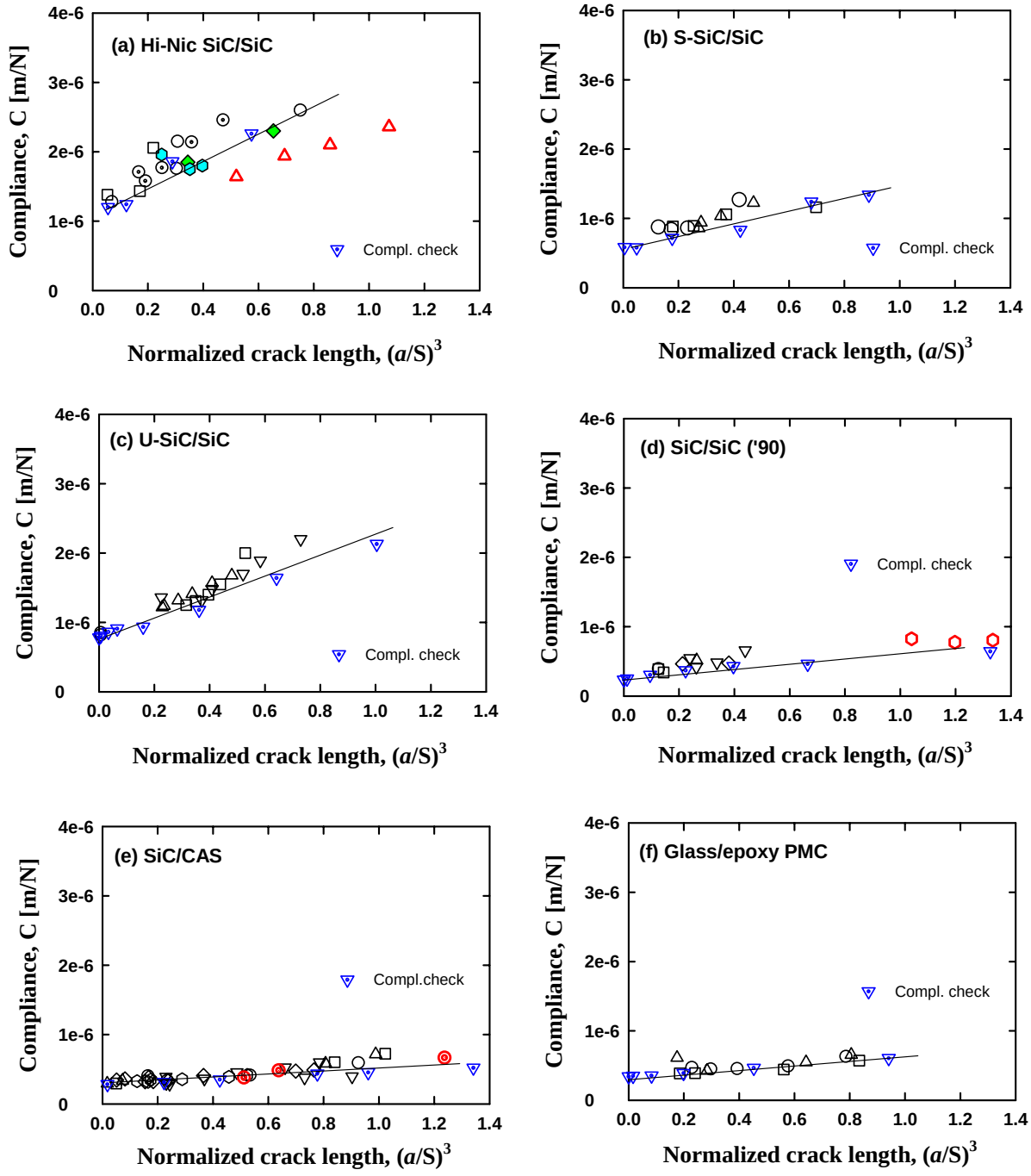

Figure 9: Comparison in compliance of ENF specimens between two different configurations of cracking in Mode I and Mode II for five different CMCs, glass/epoxy PMC, and PMMA (superglued). Mode II cracks corresponded to those propagated in Mode II tests (the data already shown in figure xx); whereas, Mode I cracks (designated “compl.check” in the figure) corresponded to those produced by Mode I wedge loading.

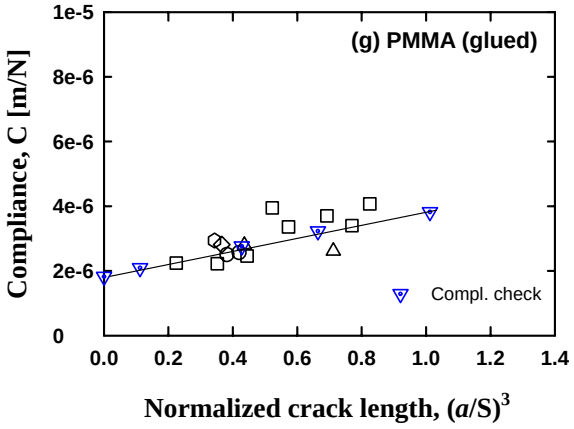

Figure 9: (Cont'd)

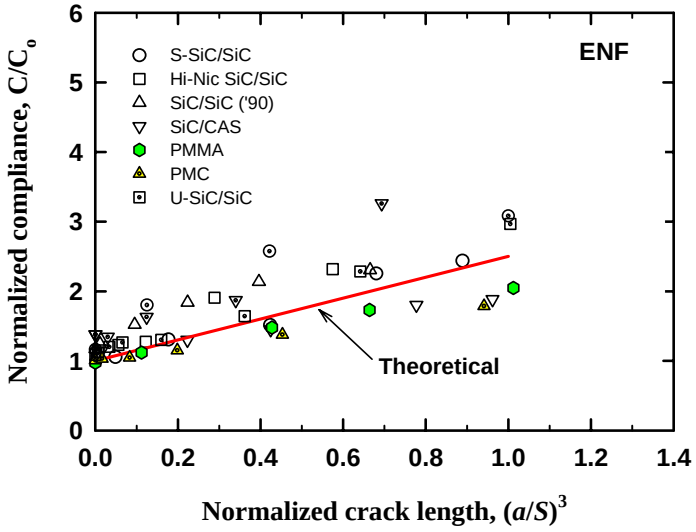

Figure 10: Normalized compliance (C/C_o) as a function of normalized crack length $(a/S)^3$ determined for five different CMCs, PMC, and PMMA (superglued) tested in Mode II. The theoretical line (Equation 7) is included.

A summary of Mode II interlaminar energy release rates G_{II} is shown in figure 11, where G_{II} was plotted as a function of normalized crack length (a/S). G_{II} was similar to G_I in terms of scatter and R-curve, as seen in the figure. All the composites exhibited rising R-curve behavior, resulting in an overall G_{II}=200-900 J/m^2. Both U-SiC/SiC and SiC/CAS composites seemed to yield greater G_{II} than other CMCs.

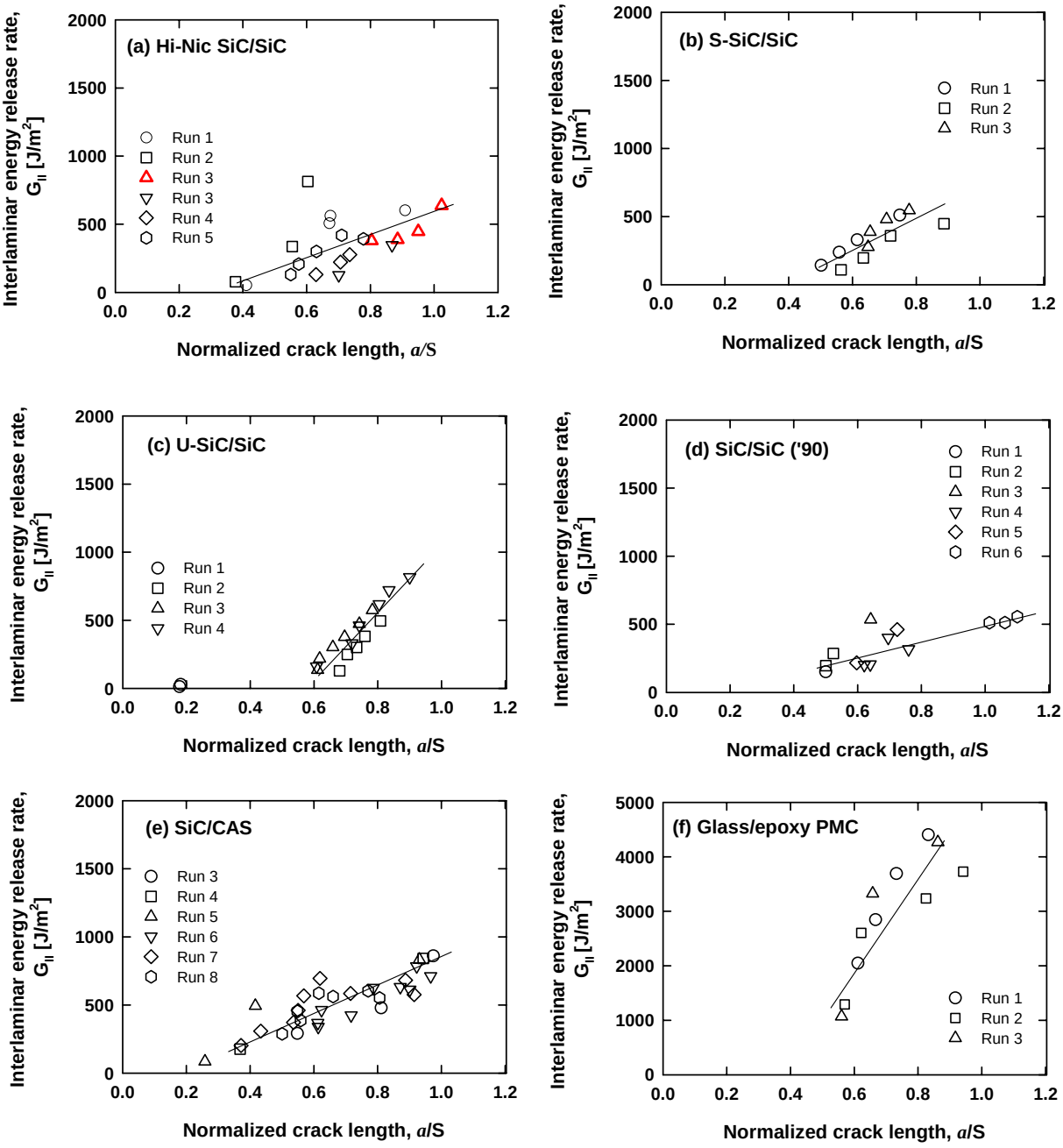

Figure 11: Mode II interlaminar energy release rate (G_{II}) as a function of normalized crack length (a/S) determined at ambient temperature by ENF in Mode II for (a) Hi-Nic SiC/SiC, (b) S-SiC/SiC, (c) U-SiC/SiC, (d) SiC/SiC ('90), (e) SiC/CAS, (f) glass/epoxy PMC, and (g) PMMA (superglued).

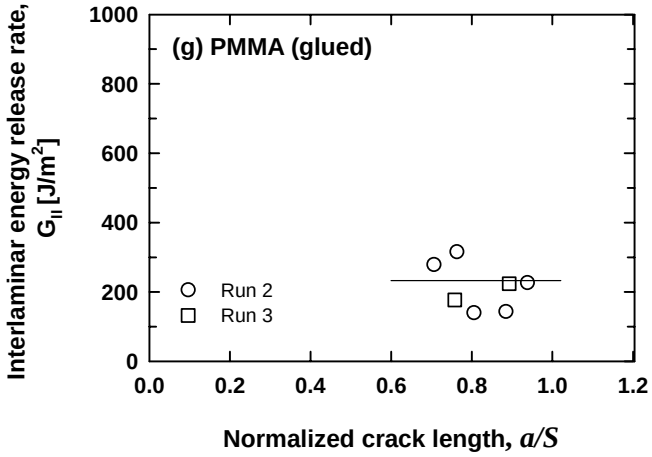

Figure 11: (Cont'd)

The glass/epoxy PMC exhibited significant G_{II} (=1000 to 4000 J/m^2) with a rising R-curve. As in Mode I, PMMA showed a flat R-curve with G_{II}≈200 J/m^2, which is around at the lower end of G_{II} for the CMCs. Despite its low G_{II}, PMMA gave a daunting challenge to carry out ENF testing of all the materials because of its frequent flexure failure.

3.4 R-CURVE BEHAVIOR

The rising R-curve behavior shown in both G_I and G_{II} would be primarily attributed to fiber bridging occurring in the wake region of a propagating crack. A repeated process of fiber bridging and subsequent fiber breakage as a crack propagated was clearly observed during Mode I testing, see figure 12 as an example. This process is believed to be operative in Mode II, though not as much as in Mode I, occurring in the interlaminar midplane of an ENF specimen through which a shear crack propagated. Furthermore, friction between *two* crack planes in the wake region of ENF specimen would take place as applied force monotonically increased and as a sliding motion occurred between the two mating crack planes because of their opposite modes of deformation. This would contribute as an added resistance to crack propagation so that more energy would be required for a crack to propagate. This phenomenon of frictional constraint was evident from fracture surfaces of ENF specimens where many broken fibers/debris were observed, as shown in figure 13. This friction-associated feature was not seen in Mode I testing, where much cleaner fracture surfaces were characterized, see figure 13.

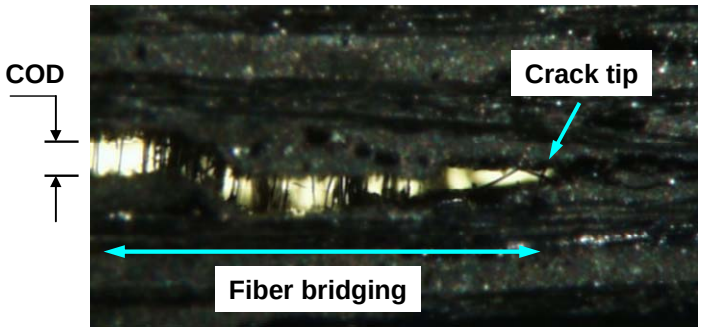

Figure 12: Typical example showing fiber bridging in the wake region of a propagating crack during Mode I DCB testing for S-SiC/SiC composite.

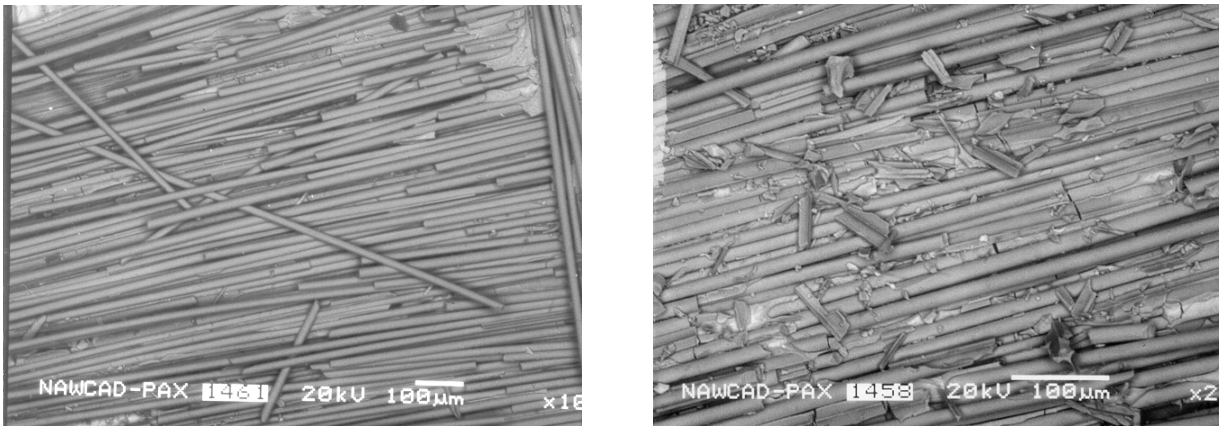

(a) (b)

Figure 13: Fracture surfaces of Hi-Nic SiC/SiC composite specimens in: (a) DCB test in Mode I and (b) ENF test in Mode II. Note the existence of broken fibers/debris in (b) due to the frictional sliding motion of two mating crack planes in an ENF specimen.

As seen before, the CMCs exhibited 1-3 times greater in G_{II} than G_I; whereas, the PMC showed 2-3 times greater in G_I. By contrast, PMMA exhibited virtually no a rising R-curve in either Mode I or II and showed no appreciable difference in G_I and G_{II} with G_I, G_{II}=200-300 J/m^2. This clearly indicates that smooth interfaces like PMMA would generate no rising R-curve or $G_{II}>G_I$. Based on these supplementary results for PMMA, the reasoning of fiber bridging and frictional constraint as rising R-curve and $G_{II}>G_I$ would be justified for the CMCs and PMC. In other words, the main reason for greater G_{II} than G_I observed in this work would be primarily due to significant frictional constraint occurring in the very *rough* wake region of a propagating crack. Some coarse-grained monolithic ceramics, when used with compression-induced test geometry (e.g., in diametral compression), exhibited such a frictional constraint, resulting in greater Mode II fracture toughness than Mode I counterpart [30]. However, this observation has not always been the case when different loading/specimen configurations such as single edge precrack or v-notched beam specimens are used [31,32].

3.5 COMPARISON OF CRACK GROWTH RESISTANCES

Figure 14 summarizes schematically G_I and G_{II} for the CMCs tested. Except for the SiC/CAS composite in G_I, there was no significant difference in overall G_I or G_{II} among the CMCs. This also indicates that either boron nitride coatings or silicon melt infiltration would not have any noticeable effect on G_I or G_{II}.

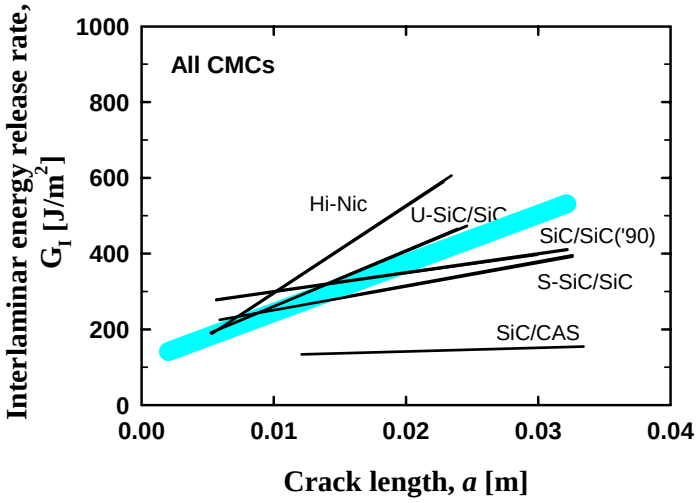

(a)

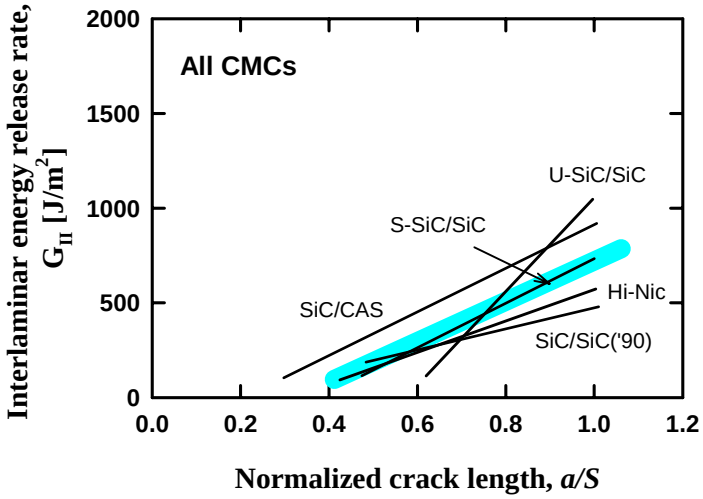

(b)

Figure 14: Summary of interlaminar energy release rates of five different CMCs tested. (a) G_I by DCB method (Mode I); (b) G_{II} by ENF method (Mode II). The thick line indicates an approximate representation of all the CMCs tested for a given mode of loading.

Figure 15 compares G_I and G_{II} as a function of crack length for the CMCs, PMC, and PMMA. Although the CMCs showed favorable rising R-curve behavior, their magnitude of G_I or G_{II} was still considerably lower than that of the glass/epoxy composite. The glass/epoxy composite exhibited almost 2-3 times greater in G_I and 8 times (when estimated at a/S=0.8) greater in G_{II} than the CMCs. The CMCs were typified of lower G_I or G_{II} when compared with the PMC, which needs to be improved to yield better interlaminar properties. It was frequently observed from fracture surfaces that fibers and matrix in some areas were not adequately adhered, showing little imprints of fibers on the matrix, as can be seen in figure 16. This lack of fiber-matrix bonding would be one major cause of poor interlaminar properties of the CMCs.

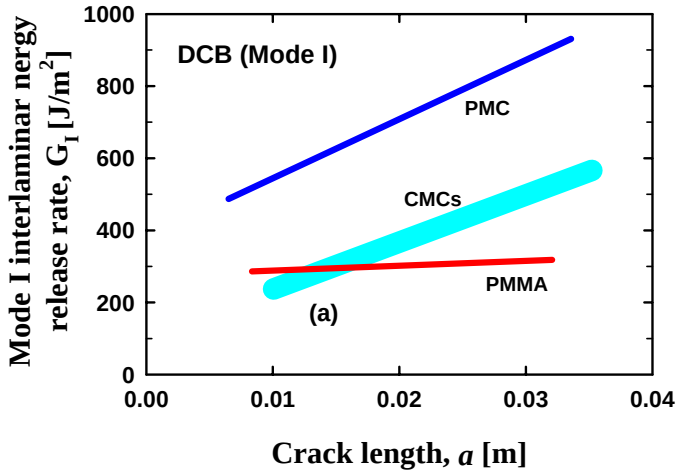

(a)

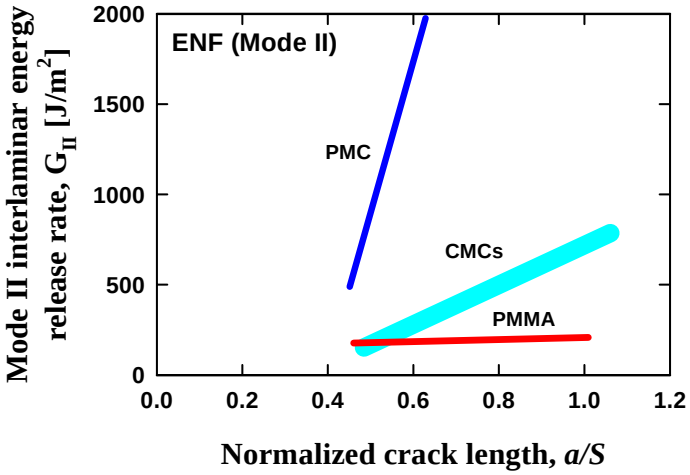

(b)

Figure 15: A simplified summary of interlaminar energy release rates of CMCs, PMC, and PMMA: (a) Mode I interlaminar energy release rate (G_I) by DCB method; (b) Mode II interlaminar energy release rate (G_{II}) by ENF method.

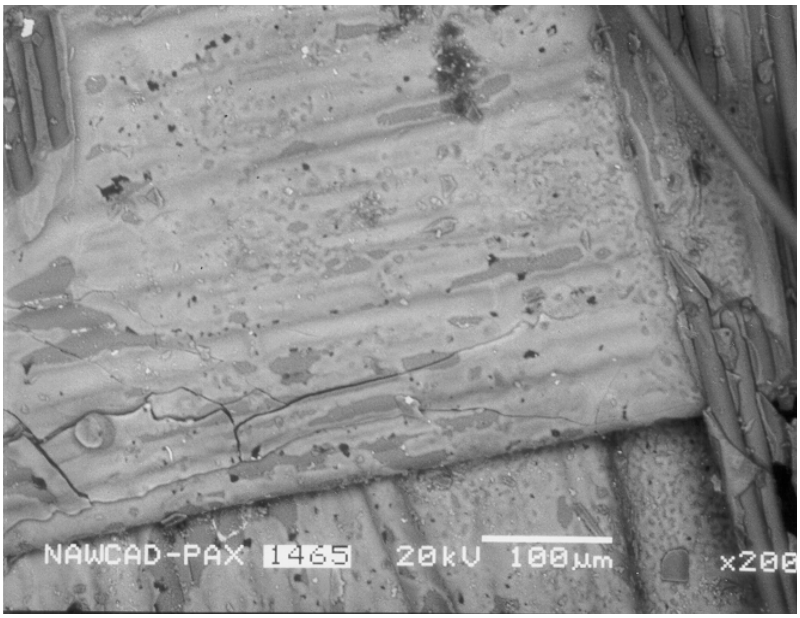

Figure 16: Fracture surface of matrix region showing limited imprints of fibers for Hi-NiC SiC/SiC composite tested in DCB in Mode I.

A previous study showed that many of the CMCs, including those used in this work, exhibited interlaminar shear strength approximately three times greater than interlaminar tensile strength [7]. The results are illustrated in figure 17, where interlaminar shear strength was plotted against interlaminar tensile strength for a total of 10 CMCs. Regardless of fiber/matrix material or architecture, CMCs exhibited an almost 3:1 ratio in interlaminar shear to interlaminar tensile strength. Analogous to strength, crack growth resistance G_{II} was also plotted against G_I for the CMCs used in this work, as shown in figure 18. Except the SiC/SiC (’90) and Hi-Nic SiC/SiC composites that yielded an 1:1 ratio, the three remaining CMCs and the PMC exhibited an approximate 3:1 relation in G_{II}/G_I, similar to the trend shown in interlaminar strengths. This may not be surprising based on Weibull statistics/fracture mechanics, considering that G_{II} was almost 1-3 times greater than G_I, and that the same flaws population would control both interlaminar shear and tensile strengths. More data on crack growth resistances, of course, are needed to better establish the crack growth resistance versus strength relation for CMCs.

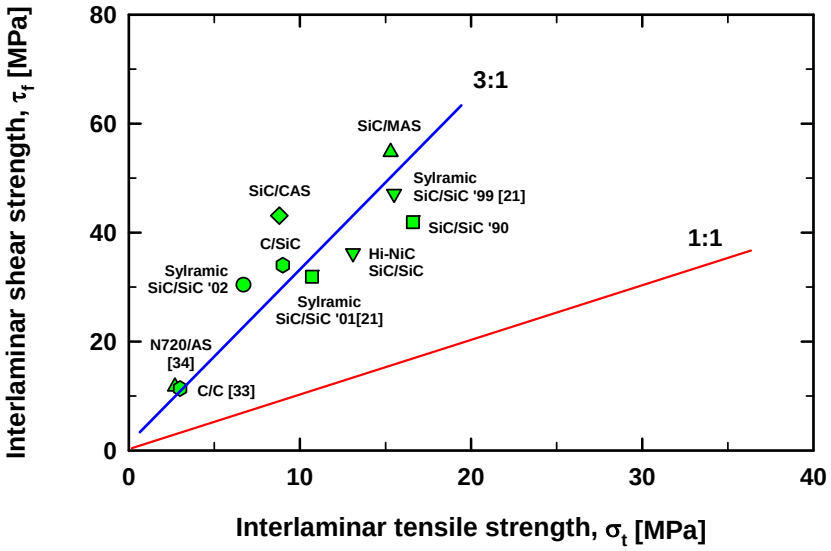

Figure 17: Comparison in interlaminar shear and interlaminar tensile strengths for various CMCs including the CMCs used in this work [7].

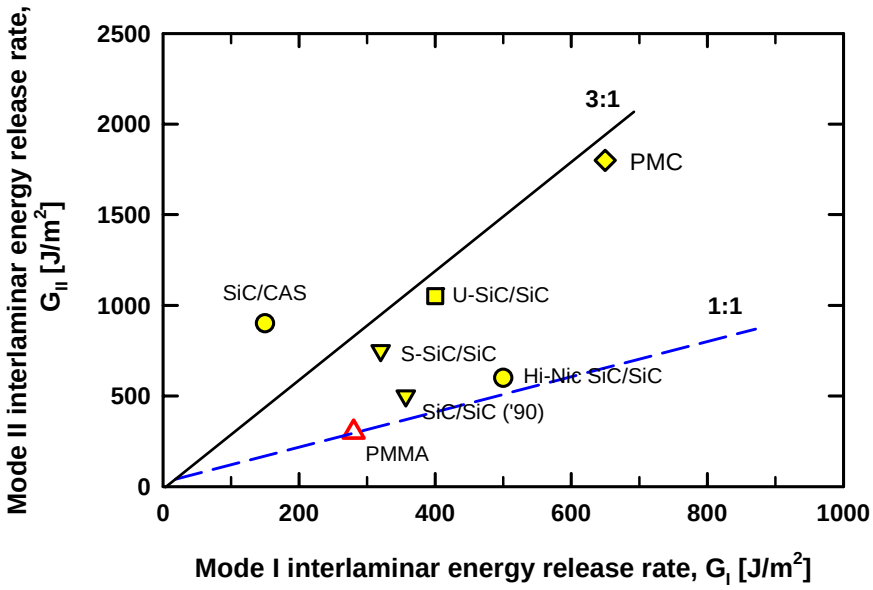

Figure 18: (a) Comparison in G_I and G_{II} for five different CMCs, PMC, and PMMA (superglued) determined in this study

3.6 EFFECT OF THE OFF-THE-CENTER OF A CRACK PLANE ON G_I AND G_{II}

The scatter of data on G_I and G_{II} observed in this work may have two major plausible sources: the materials' microscopic inhomogeneity and the experimental errors. The former is inherent and beyond the scope of this work to explore in details. The latter, the experimental errors, may come from several factors such as force and crack length measurements and test specimen' dimensional inaccuracy. Two main sources of the experimental errors are believed to be associated with the crack length measurements and the preparation of a crack at the midplane of a test specimen. It was experienced that to produce a precrack at the midplane, that is, $h_1=h_2=h$, was a more daunting task than the crack length measurements, mainly due to rough, as-fabricated surfaces of test specimens (surface machining, if applied, may cause possible damage to fiber/matrix architecture). Moreover, in some cases, a crack propagated along the midplane but then deviated from the midplane. Therefore, it is worthy to estimate quantitatively the effect of $h_1 \neq h_2$ on G_I and G_{II}.

The total energy release rate G_{Id} of a DCB test specimen with $h_1 \neq h_2$ (see figure 2) is a summation of G_{I1} and G_{I2} [35]

$$\begin{aligned} G_{Id} &= G_{I1} + G_{I2} \\ &= \frac{a^2 P^2}{2Eb}\left[\frac{1}{I_1} + \frac{1}{I_2}\right] \\ &= \frac{6a^2 P^2}{Eb^2 h_2^3}\left[\frac{1+\gamma^3}{\gamma^3}\right] \end{aligned} \tag{8}$$

where

$$\gamma = \frac{h_1}{h_2} \tag{9}$$

and I_1 and I_2 are the second moment of inertia of each cantilever arm about its neutral axis. The above equation can be easily derived from the simple beam theory together Equation (1). This equation is fundamentally the same as Equation (3) but in a different form. The term outside the bracket represents G_I for the case of $h_1=h_2=h$. Therefore, the ratio of G_{Id} to G_I, noting $h_1+h_2=2h$, is simply

$$\frac{G_{Id}}{G_I} = \frac{1}{16}(\gamma+1)^3\left[\frac{1+\gamma^3}{\gamma^3}\right] \tag{10}$$

Note that when $h_1=h_2$, Equation (10) reduces to $G_{Id}/G_I=1$.

In the same way, the ratio of G_{IId}/G_{II} can be derived based on the simple beam theory. Beam deflections are considered in three different sections of AB, BC, and CD (see figure 2(b)) with a condition of $h_1 \neq h_2$. The total deflection δ at the load point of the beam is a summation of deflections associated with sections AB, BC, and CD. Using the beam theory, neglecting the shear deformation, deflection of each section can be derived as follows:

$$\delta_{AB} = \frac{aP}{4E}\left[\frac{a^2}{3I_2}\left(\frac{1}{1+I_1/I_2}\right)+\frac{1}{2I}(S^2-a^2)\right] \tag{11}$$

$$\delta_{BC} = \frac{P}{24EI}[2S^3-3aS^2+a^3] \tag{12}$$

$$\delta_{CD} = \frac{PS^3}{12EI} \tag{13}$$

where I is the second moment of inertia of the uncracked sections (BC and CD). Using $\delta=\delta_{AB}+\delta_{BC}+\delta_{CD}$ and Equations (1) and (2) with some mathematical manipulations yield a solution of G_{IId} for $h_1 \neq h_2$ as follow:

$$G_{IId} = -\frac{3a^2P^2}{16Eb^2h^3}+\frac{3a^2P^2}{2Eb^2h_2^3}\left[\frac{1}{1+\gamma^3}\right] \tag{14}$$

When $h_1=h_2=h$, Equation (14) can be reduced to G_{II} as

$$G_{II} = \frac{9a^2P^2}{16Eb^2h^3} \tag{15}$$

which is identical to Equation (4) after a substitution of $C=(2S^3+3a^3)/8Ebh^3$ in Equation (4) [13,14]. Therefore, the ratio of G_{IId}/G_{II}, noting $h_1+h_2=2h$, becomes

$$\frac{G_{IId}}{G_{II}} = -\frac{1}{3}+\frac{1}{3}(\gamma+1)^3\left(\frac{1}{1+\gamma^3}\right) \tag{16}$$

When $h_1=h_2$, Equation (16) reduces to $G_{IId}/G_{II}=1$.

The effect of h_1/h_2 on G_I or G_{II} can be now estimated using Equation (10) or (16). Equations (10) and (16) are illustrated in figure 19. In order to have a 5% error in G_I and G_{II}, for example, the variation of h_1 with respect to h_2 (and *vice versa*) should be within 17-20% for G_I; whereas the variation should be within 20-25% for G_{II}. This indicates that to have a negligible error ($\leq$5%) in G_I or G_{II}, $h1$ and h2 should remain within about 20% in tolerance to each other. In fact, this would be a relatively large allowance since the variation in h_1 or h_2 was observed much less than 20% from the experiments. Therefore, it is believed that practically the effect of h_1/h_2 on G_I or G_{II} appears to be minimal and that the major variation, discrepancy, or data scatter would have been associated with materials' inherent microscopic inhomogeneity.

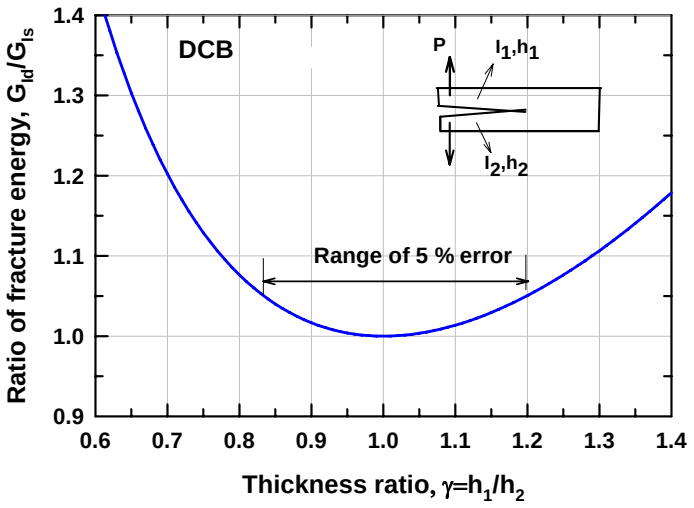

(a)

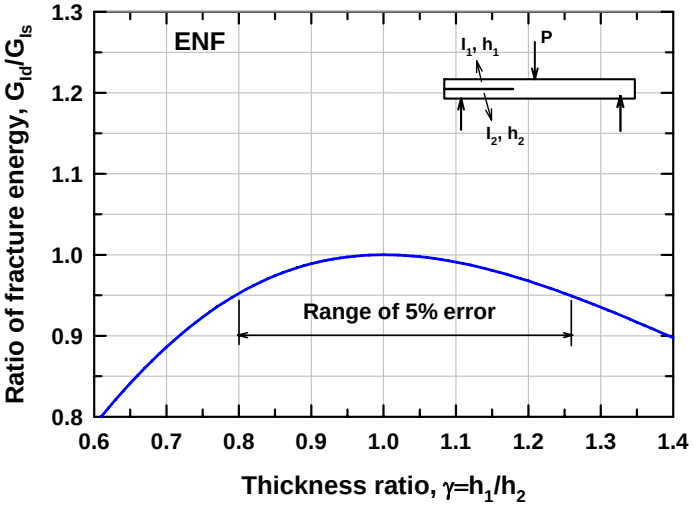

(b)

Figure 19: Ratio of energy release rate (G_d/G) as a function of thickness ratio of h_1/h_2: (a) DCB test and (b) ENF test, showing an error due to the off-the-center of a midcrack plane. I_1 or I_2 indicates the second moment of inertia of each of two cantilever beams.

4. CONCLUSIONS

1. Interlaminar crack growth resistances were in a range of G_I=200-500 J/m^2 and G_{II}=200-900 J/m^2 for all the CMCs tested.

2. G_I was greatest for the Hi-Nic SiC/SiC composites and appeared to be similar for the other SiC/SiC composites. Both U-SiC/SiC and SiC/CAS composites seemed to yield greater G_{II}.than the other composites. Neither MI nor BN coating had a significant effect on G_I or G_{II}.

3. The CMCs, except SiC/CAS in Mode I, exhibited rising *R*-curve behavior in both G_I and G_{II}, attributed to fiber bridging in Modes I and II and frictional constraint in Mode II. The frictional constraint occurring in ENF test specimens might have yielded greater G_{II} than G_I.

4. The variation in crack midplane showed only a minor effect on G_I or G_{II}: 20% variation in h_1 or h_2 resulted in only 5% error in G_I or G_{II}.

5. The glass/epoxy PMC exhibited significantly greater G_I (2-3 times) and G_{II} (8 times) than the CMCs.

THIS PAGE INTENTIONALLY LEFT BLANK

REFERENCES

1. P. Brondsted, F. E. Heredia, and A. G. Evans, "In-Plane Shear Properties of 2-D Ceramic Composites," *J. Am. Ceram. Soc*., **77**[10] 2569-2574 (1994).

2. E. Lara-Curzio and M. K. Ferber, "Shear Strength of Continuous Fiber Ceramic Composites," ASTM STP 1309, p. 31, American Society for Testing and Material, West Conshohocken, PA (1997).

3. N. J. J. Fang and T. W. Chou, "Characterization of Interlaminar Shear Strength of Ceramic Matrix Composites," *J. Am. Ceram. Soc*., **76**[10] 2539-2548 (1993).

4. Ö. Ünal and N. P. Bansal, "In-Plane and Interlaminar Shear Strength of a Unidirectional Hi-Nicalon Fiber-Reinforced Celsian Matrix Composite," *Ceramics International*, **28** 527-540 (2002).

5. S. R. Choi and N. P. Bansal, "Shear Strength as a Function of Test Rate for SiC_f/BSAS Ceramic Matrix Composite at Elevated Temperature," *J. Am. Ceram. Soc*., **87**[10] 1912-1918 (2004).

6. S. R. Choi, N. P. Bansal, A. M. Calomino, and M. J. Verrilli, "Shear Strength Behavior of Ceramic Matrix Composites at Elevated Temperatures," *Advances in Ceramic Matrix Composites X*, Edited by J. P. Singh, N. P. Bansal, and W. M. Kriven, The American Ceramic Society, Westerville, Ohio; *Ceramic Transactions*, **165** 131-145 (2005).

7. S. R. Choi and N. P. Bansal, "Interlaminar Tension/Shear Properties and Stress Rupture in Shear of Various Continuous Fiber-Reinforced Ceramic Matrix Composites," *Advances in Ceramic Matrix Composites XI*, edited by N. P. Bansal, J. P. Singh, and W. M. Kriven, The American Ceramic Society, Westerville, Ohio; *Ceramic Transactions*, **175** 119-134 (2006).

8. H. M. Yun and J. A. DiCarlo, "Through-Thickness Properties of 2D Woven SiC/SiC Panels with Various Microstructures," *Ceram. Eng. Sci. Proc*., **25**[4] 71-78 (2004).

9. L. P. Zawada, "Longitudinal and Transthickness Tensile Behavior of Several Oxide/Oxide Composites," *Ceram. Eng. Sci. Proc*., **19**[3] 327-339 (1998).

10. E. Lara-Curzio, D. Bowers, and M. K. Ferber, "The Interlaminar Tensile and Shear Behavior of a Unidirectional C-C Composite," *J. Nucl. Mater*., **230** 226-232 (1996).

11. S. Mall, R. P. Vozzola, and L. Zawada, "Characterization of Fracture in Fiber-Reinforced Ceramic Composites under Shear Loading," *J. Am. Ceram. Soc*., **72**[7] 1175-1178 (1989).

12. R. H. Martin, "Delamination Characterization of Woven Glass/Polyester Composites," *J. Comp. Tech. and Research*, **19**[1] 20-28 (1977).

13. N. Sela and O. Ishai, "Interlaminar Fracture Toughness and Toughening of Laminated Composite Materials: Review," *Composites*, **20**[5] 423-435 (1989).

14. L. A. Carlsson, J. W. Gillespie, and R. B. Pipes, "On the Analysis and Design of the End Notched Flexure (ENF) Specimen for Mode II Testing," *J. Comp. Mater*., **20** 594-604 (1986).

15. T. K. O'Brien and R. H. Martin, "Round Robin Testing for Mode I Interlaminar Fracture Toughness of Composite Materials," *J. Comp. Tech. and Research*, **15**[4] 269-281 (1993).

16. J. G. Williams, "The Fracture Mechanics of Delamination Tests," *J. Strain Analysis*, **24**[4] 207-214 (1989).

17. D.V.T.G.P. Kumar and B.K.R. Prasad, "Higher-Order Beam Theories for Mode II Fracture of Unidirectional Composites," *J. Appl. Mechanics*, Transaction of the ASME, **70** 840-852 (2003).

18. A. J. Smiley and R. B. Pipes, "Rate Effects on Mode I Interlaminar Fracture Toughness in Composite Materials," *J. Comp. Mater*., **21** 670-687 (1987).

19. S. R. Choi and R. W. Kowalik, "Interlaminar Crack Growth Resistances of Various Ceramic Matrix Composites in Mode I and Mode II Loading," ASME Paper No. GT2007-27080, *Proceedings of ASME Turbo Expo 2007*, 14-17 May 2007, Montreal, Canada (to be presented).

20. D. Brewer, "HSR/EPM Combustor Materials Development Program," *Mat. Sci. Eng.*, **A261** 284-291 (1999).

21. A. M. Calomino, "Mechanical Behavior and Characterization/1316^{o}C In-Situ BN Coated MI/SiC/SiC," Technology Forum, UEET, Glenn Research Center, National Aeronautics and Space Administration, Cleveland, Ohio, Oct 2002.

22. ASTM C 1259, "Test Method for Dynamic Young's Modulus, Shear Modulus, and Poisson's for Advanced Ceramics by Impulse Excitation of Vibration," *Annual Book of ASTM Standards*, Vol. 15.01, American Society for Testing and Materials, West Conshohocken, PA (2006).

23. D. W. Worthem, "Thermomechanical Fatigue Behavior of Three CFCCs," NASA CR-195441, National Aeronautics and Space Administration, Glenn Research Center, Cleveland, OH (1995).

24. S. R. Choi and J. P. Gyekenyesi, "Load-Rate Dependency of Ultimate Tensile Strength in Ceramic Matrix Composites at Elevated Temperatures," *Int. J. Fatigue*, **27** 503-510 (2005).

25. S. R. Choi, R. T. Bhatt, J. M. Pereira, and J. P. Gyekenyesi, "Foreign Object Damage Behavior of a SiC/SiC Composite at Ambient and Elevated Temperatures," *ASME Paper No*. GT2004-53910 (2004).

26. ASTM D 5528, "Test Method for Mode I Interlaminar Fracture Toughness of Unidirectional Fiber-Reinforced Polymer Matrix Composites," *Annual Book of ASTM Standards*, Vol. xxx American Society for Testing and Materials, West Conshohocken, PA (2005).

27. A. A. Volinsky, N. R. Moody, and W. W. Gerberich, "Overview: Interfacial Toughness Measurements for Thin Films on Substrates," *Acta Materialia*, **50** 441-466 (2002).

28. L. L. Shaw, B. Barber, E. H. Jordan, and M. Gell, "Measurements of the Interfacial Fracture Energy of Thermal Barrier Coatings," *Scripta Materialia*, **39**[10] 1427-1434 (1998).

29. See any text, e.g., D. Broek, Elementary Engineering Fracture Mechanics, Ch 5, Martinus Nijhoff Publishers, Boston (1983).

30. D. Singh and D. K. Shetty, "Fracture Toughness of Polycrstalline Ceramics in Combined Mode I and Mode II loading," *J. Am. Ceram. Soc*., **72**[1] 78-84 (1989).

31. V. Tikare and S. R. Choi, "Combined Mode I and Mode II Fracture of Monolithic Ceramics," *J. Am. Ceram. Soc*., **76**[9] 2265-72 (1993).

32. S. R. Choi, D. Zhu, and R. A. Miller, "Mixed-Mode Fracture Behavior of Ceramic Plasma-Sprayed Thermal Barrier Coatings at Ambient and Elevated Temperatures," *Engineering Fracture Mechanics*, **72** 2144-2158 (2005).

33. E. Lara-Curzio, D. Bowers, and M. K. Ferber, "The Interlaminar Tensile and Shear Behavior of a Unidirectional C-C Composite," *J. Nucl. Mater*., **230** 226-232 (1996).

34. L. P. Zawada, "Longitudinal and Transthickness Tensile Behavior of Several Oxide/Oxide Composites," *Ceram. Eng. Sci. Proc*., **19**[3] 327-339 (1998).

35. H. Tada, P.C. Paris, and G. R. Irwin, The Stress Analysis of Cracks Handbook, p. 418, ASME, NY (2000).

THIS PAGE INTENTIONALLY LEFT BLANK

DISTRIBUTION:

NAVAIRWARCENACDIV (4.3.4.1/Choi), Bldg. 2188, Room 101A (10)
48066 Shaw Road, Patuxent River, MD 20670
NAVAIRSYSCOM (AIR-5.1), Bldg. 304, Room 100 (1)
22541 Millstone Road, Patuxent River, MD 20670-1606
NAVAIRSYSCOM (AIR-4.0X), Bldg. 407, Room 116 (1)
22269 Cedar Point Road, Patuxent River, MD 20670-1120
NAVTESTWINGLANT (55TW01A), Bldg. 304, Room 200 (1)
22541 Millstone Road, Patuxent River, MD 20670-1606
DTIC (1)
Suite 0944, 8725 John J. Kingman Road, Ft. Belvoir, VA 22060-6218